PAPER

Thermal conductivity of defective graphene: an efficient molecular dynamics study based on graphics processing units

IOP Publishing Nanotechnology
Nanotechnology 31 (2020) 215708 (9pp) https://doi.org/10.1088/1361-6528/ab73bc

Thermal conductivity of defective graphene: an efficient molecular dynamics study based on graphics processing units

Xin Wu and Qiang Han

Department of Engineering Mechanics, School of Civil Engineering and Transportation, South China University of Technology, Guangzhou, Guangdong Province 510640, People's Republic of China

E-mail: emqhan@scut.edu.cn

Received 5 December 2019, revised 27 January 2020
Accepted for publication 6 February 2020
Published 10 March 2020

Abstract

The exceptional thermal transport properties of graphene are affected due to the presence of various topological defects, which include single vacancy, double vacancies and Stone–Wales defects. The present article is intended to study on thermal transport properties of defective graphene by comparing the effects of topological defects on the thermal conductivity of graphene. This study developed a program for constructing defective graphene models with customizable defect concentrations and distribution types. The efficient molecular dynamics method based on graphics processing units is applied, which can achieve efficient and accurate calculation of material thermal conductivity. It is revealed that the existence of topological defects has a considerable reduce on the thermal conductivity of graphene, and the declining rate of the value get less with increasing defects concentration. At the same concentration, the weakening effect of SW defects on the thermal conductivity of graphene is evidently less than the other two defects. We also explored the effect of temperature on the thermal conductivity of graphene with different defects. These findings were discussed from the phonon perspective that elucidate the atomic level mechanisms, which provide guidance for thermal management of graphene devices.

Keywords: thermal conductivity, defective graphene, molecular dynamics, graphics processing units

(Some figures may appear in colour only in the online journal)

1. Introduction

With the rapid development of the micro-nano technology, the materials used in microelectronics, bioengineering, radiation sources and detectors are gradually entering micro-nano scale [1–3]. The miniaturization of equipment causes sharply rise of its heat energy density, which takes the thermal transport problem to be of vital importance. Due to the limitation of charge and thermal transport in the out-of-plane direction, two-dimensional (2D) materials present much abnormal physical phenomena [4–10]. Graphene, the most representative carbon-based 2D material, has been prepared by mechanical stripping of pyrolytic graphite in 2004 [11]. Depend on the special structure and bonding mode, graphene is endowed with excellent electrical, thermal and mechanical properties [12–14], which has broad application prospects.

Raman spectroscopy results have shown that the pristine suspended graphene has an exceptionally high thermal conductivity of up to about 1800–5300 $W\,mK^{-1}$ at room temperature [15–17], typically 2500 $W\,mK^{-1}$ as the reports. The wide range is caused by experimental measurement errors of Raman spectroscopy and uncertainty of sample conditions. In sharp contrast, the thermal conductivity of silver, the metal with excellent thermal transport performance in nature world, is only about 430 $W\,mK^{-1}$. However, it is almost impossible to prepare large-sized pristine graphene based on the existing preparation technology of graphene, such as chemical vapor deposition, mechanical stripping and epitaxial growth method

[11, 18, 19]. In graphene structures, the presence of defects is unavoidable, such as vacancies, dislocations and grain boundaries. Simultaneously, defect engineering is one of the most common and effective means in regulating the properties of materials to suit different application conditions [20]. Therefore, a clear understanding of the effects of various defects on the thermal transport properties of graphene is of great significance for the design of nanomaterials.

At present, there are two main classical molecular dynamics simulation methods for calculation of thermal conductivity of nanomaterials [21, 22]: non-equilibrium molecular dynamics method (NEMD) [23–25] based on Fourier equation and equilibrium molecular dynamics method (EMD) [26] based on Green–Kubo equation. large-scale atomic/molecular massively parallel simulator (LAMMPS) software package [27], a quite popular large-scale molecular dynamics simulation software package, is often used to simulate and calculate the thermal conductivity of nanomaterials. Ghasemi *et al* [23] studied the regulation mechanism of pore topology engineering on graphene thermal conductivity. Based on the AIREBO potential function, the thermal conductivity of pristine graphene is calculated as 121.2 $W\,mK^{-1}$ in their study. In the work of studying the effect of vacancy defects on the thermal conductivity of carbon-based nanomaterials by Liu *et al* [24], the calculated thermal conductivity of the pristine graphene based on the Tersoff potential is only $74.10 \pm 1.85\,W\,mK^{-1}$. Under the same potential function, Wei *et al* [25] calculated the thermal conductivity of the pristine graphene after linear extrapolation to eliminate the size effect, which is only 870 $W\,mK^{-1}$. The ReaxFF potential was also used to evaluate the thermal conductivity of carbon-based materials [28, 29], which is superior to AIRBEO potential in thermal conductivity simulation of graphene. Diao *et al* [30] obtained an overall extrapolation of graphene thermal conductivity of 1390 $W\,mK^{-1}$. It is within the lower limit of the value measured by the Raman photothermal method. In the EMD method with negligible size effect, Maliha *et al* [26] used the REBO potential to calculate the thermal conductivity of the graphene nanoribbons as 900 $W\,mK^{-1}$. It is not difficult to find that these results are far from the experimental results.

Limited by size effect and inaccuracy in describing the empirical potential, the calculation results by NEMD method are often not accurate enough. Although the size effect can be negligible in EMD method, the heat flow formula used in the LAMMPS is only applicable to two-body potentials such as Lennard-Jones argon and is not suitable for describing many-body systems such as graphene and carbon nanotubes [31, 32]. This is reflected in the above calculation as an underestimation of thermal conductivity. Under these circumstances, the reliability of the results of the above studies on the thermal transport properties of the graphene containing defects is bound to be affected.

From another perspectivity, the large-scale and complicated system is an irreversible trend in the development of computer simulation. In the case of ensuring the accuracy of the simulation, it is one of the goals of the development of analog technology to increase the speed of calculation as much as possible. For classical molecular dynamics simulations, its computational characteristics are well suited for massively parallel computing. Therefore, the intervention of the graphics processing units (GPU) acceleration architecture is very beneficial to it [33].

The present article is based on an efficient molecular dynamics code implemented on GPU and numerically simulated by EMD method. The precise heat flow formula is applied to avoid underestimating the thermal conductivity of materials while the GPU acceleration architecture can greatly improve the computational efficiency [34]. In this article, the graphene thermal transport properties with three different topological defects (single vacancy, double vacancies and Stone–Wales defects) is studied. The differences of thermal transport properties among three above kinds of defective graphene and the reasons for these differences are also analyzed from the phonon perspective. The performance of thermal conductivity of defective graphene at different temperatures was also studied, which is a pivotal factor affecting lattice vibration and phonon states. And we discussed the possible constraints on the thermal conductivity of graphene due to defects and temperature.

2. Model and method

As shown in figure 1(a), the research object is a square monolayer graphene with an in-plane length of $20\,nm \times 20\,nm$. Square samples are more suitable for EMD simulations due to the same size in both chiral directions of graphene. There are three common topological defects of graphene: single vacancy, double vacancies and Stone–Wales (SW) defects. The loss of a single carbon atom and two adjacent carbon atoms introduces a single atom vacancy and a diatomic vacancy defect, respectively as identified in figures 1(b)–(d) And the SW defects in figure 1(d) are obtained by rotating two adjacent carbon atoms 90° around their center point. In this process, the four hexagonal rings have become two pentagonal rings and two heptagonal rings. Hence, it is also called 5-7-7-5 defect, which is the most common of the graphene topological defects.

The defect concentration is defined as the ratio of the number of non-hexagonal rings in the defective graphene with respect to the total number of hexagons in the initial pristine sheet. Algorithms specifically designed for modeling are developed, which can realize the construction of a randomly distributed defective graphene model with specified defect types and concentrations. The randomness of the defect distribution includes the overall positional randomness and the randomness of the respective orientations. As schematically shown in figures 1(b)–(d), in the direction indicated by the arrow, the single vacancy defect has two orientation modes, which is determined by the particularity of the atomic position in the graphene honeycomb structure. The difference of orientation in the other two defects is determined by the relative positions of two adjacent carbon atoms forming defects, which can be characterized by the orientation of carbon–carbon bonds. In the regular hexagonal carbon ring

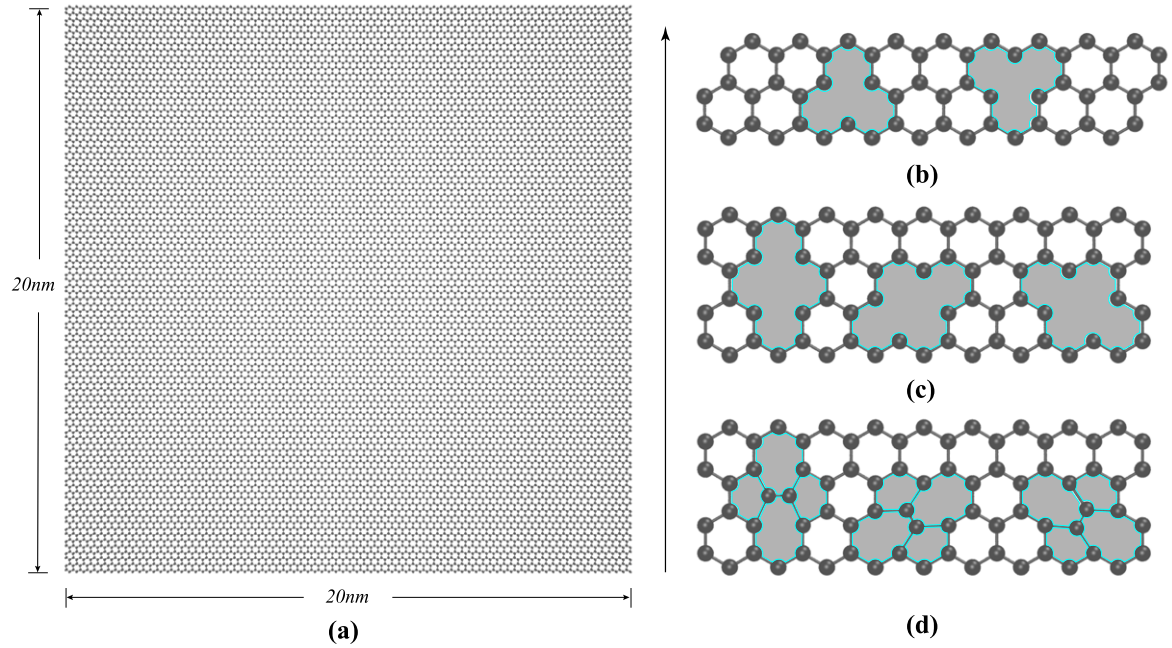

Figure 1. Schematic illustration of the configuration of graphene and its three types of topological defects: (a) square pristine monolayer graphene sheet configuration with size of 20 nm × 20 nm; (b) schematic diagram of single vacancy defects containing two different orientations; (c) schematic diagram of double vacancies defects containing three different orientations; (d) schematic diagram of SW defects containing three different orientations, which are relative to the direction of the black arrow in the figure. (The illustrated defects are schematic diagrams of the model, and carbon atoms bonding may occur during the actual simulation, especially in the vacancy defects.)

structure, there are three kinds of orientations of carbon–carbon bonds along the same direction, and thus three ways are possible for orienting double vacancies and SW defects. There is no doubt that defective graphene with such a random distribution of defects will be more reasonable.

EMD method is adopted to evaluate the thermal transport properties of defective graphene in present paper. Compared with the NEMD method, the size effect of the EMD method is minimized to obtain more accurate calculation results, and the equilibrium state simulation system is relatively stable. NEMD method is based on Fourier theorem $\kappa = J/\nabla T$, in which J represent heat flux and ∇T is the temperature gradient of area with heat flow. Usually due to the limitation of calculation cost, the size of the simulated sample is much smaller than the mean free path of the phonon, which will cause additional phonon scattering and thus underestimate the thermal conductivity of the material. The thermal conductivity of materials calculated by the EMD method is mainly based on the Green–Kubo formula [35, 36], which relates the transport coefficient of the non-equilibrium process to the fluctuation of the corresponding physical quantity in the equilibrium state. For the thermal transport process, the thermal conductivity tensor of materials $\kappa_{\alpha\beta}(t)(\alpha, \beta = x, y, z)$ during a given time equals to the integral of the heat current auto-correlation function (HCACF):

$$\kappa_{\alpha\beta}(t) = \frac{1}{k_B T^2 V} \int_0^t \langle J_\alpha(0) J_\beta(t') \rangle dt', \tag{1}$$

where k_B is the Boltzmann constant, T is the simulation temperature, V is the volume of the system. For a two-dimensional graphene sheet, its volume is defined as the product of surface area and thickness of 0.335 nm. The angle brackets in the formula represent the time origin average. In the statistical mechanics, $\langle J(0)J(t)\rangle$ is defined as HCACF with correlated time of t. J is the heat flux, which is defined as the time derivative of energy density moment:

$$\mathbf{J} = \frac{d}{dt} \sum_i \mathbf{r}_i E_i, \tag{2}$$

where $\mathbf{r}_i$ and E_i is the position vector and total energy of the atom i, respectively.

For monolayer graphene sheet described by many-body potentials, the heat flow vector including the kinetic energy term and the potential energy term is described as:

$$\mathbf{J} = \mathbf{J_K} + \mathbf{J_P} = \sum_i \mathbf{v}_i E_i + \sum_i \sum_{j \neq i} \mathbf{r}_{ij} \left(\frac{\partial U_j}{\partial \mathbf{r}_{ji}} \cdot \mathbf{v}_i \right), \tag{3}$$

where $\mathbf{v}_i$ is the velocity vector of atom i; $\mathbf{r}_{ij}$ and $\mathbf{r}_{ji}$ is the position vector between atom i and j; U_i is the potential energy of atom i.

Since the LAMMPS is not suitable for describing the many-body potentials of graphene in the heat current calculation formula [31], the GPU-accelerated molecular dynamics software package based on the above heat flow calculation formula [34] is adopted. In the classical molecular dynamics simulation, the selection of the potential function of the system is the key to the quality of the simulation. The Tersoff potential with a parameter set optimized by Lindsay and Broido [37] is used to describe the interaction among carbon atoms. It significantly improves the consistency between

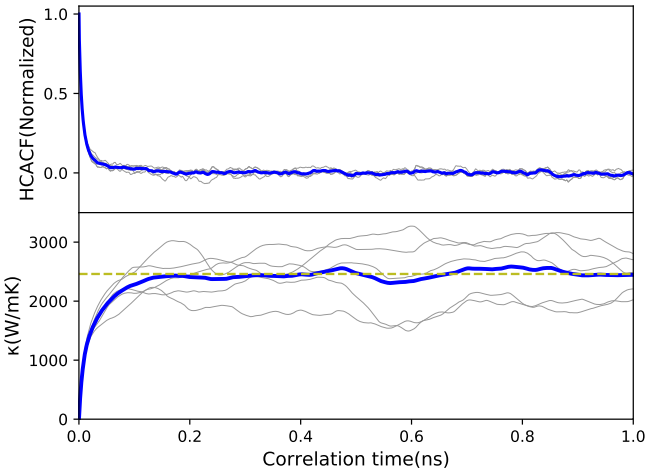

Figure 2. Normalized heat current auto-correlation function and thermal conductivity as a function of correlation time for pristine graphene with size of 20 nm × 20 nm (The solid black line represents the result of five independent simulations, and their average is plotted by the blue one. Green dotted line is the convergence reference line with the value of $\kappa = 2460\ \mathrm{W\,mK^{-1}}$.)

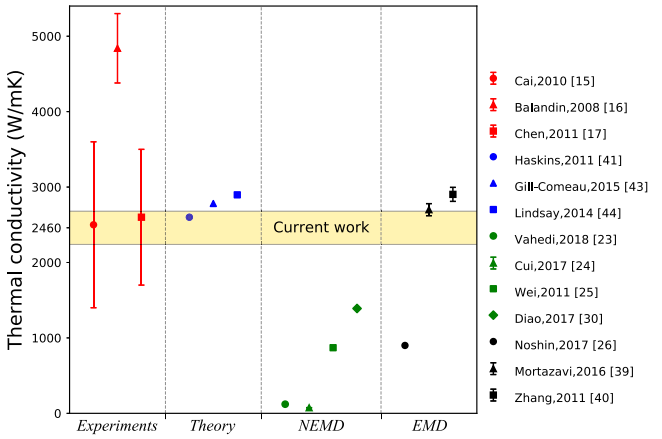

Figure 3. Results of thermal conductivity of monolayer pristine graphene at room temperature; these include experimental results based on Raman spectroscopy measurements, theoretical results based on Einstein's formula [41] and Boltzmann transport equation [43, 44], and molecular dynamics numerical calculation results based on NEMD and EMD methods. (The golden shaded part is the calculation result of this research, which can fit the experimental, theoretical and existing molecular dynamics results well.)

graphene thermal conductivity calculation and experimental measurements, and can represent its lattice dynamics and phonon thermal transfer properties more accurate [38].

In this study, periodic boundary conditions were applied in both directions of the graphene plane, which can eliminate the influence of free atoms on the boundary to minimize the size effect; and applied free boundary condition in the out-of-plane direction. For each set of simulations, the Berendsen thermostat was used at a given temperature to relax the system under the NVT ensemble for 1 ns. After the system was in a relatively stable state, a simulation of up to 10 ns was performed under the NVE ensemble, and the relevant physical quantities required for the calculation were extracted simultaneously. In order to obtain the results with better convergence, we have carried out several simulations of graphene samples with different configurations.

3. Results and discussion

We first performed the thermal conductivity calculation based on the EMD method using a pristine graphene of 20 nm × 20 nm as a sample, which contains 15228 carbon atoms. It is intended to illustrate the reliability of the simulation method by comparing the results of the calculation with the experiments and theories. In each independent simulation, the thermal conductivity results for square graphene are defined as the average of the thermal conductivity in both directions of the plane. In this part, we performed five independent simulations in a time step of 1*fs*, which is small enough for pristine graphene. The initial velocity of the atoms in each simulation was randomly given according to the ambient temperature of 300 K. The converging thermal conductivity of the pristine graphene sample can be evaluated by averaging the five sets of results. In figure 2, we calculated the convergence value of the monolayer pristine graphene thermal conductivity of $2460 \pm 220\ \mathrm{W\,mK^{-1}}$, where the error estimate is calculated by the standard error of the five independent results. The upper part of figure 2 is the normalized HCACF results of the above graphene sheet. With the results, we calculated its thermal conductivity, which converges well in the correlation time of 1 ns.

As shown in figure 3, it is within the range of experimental results [15–17], and almost equal to the existing simulation results [25, 39, 40] and the theoretical results [41, 42] of $2600\ \mathrm{W\,mK^{-1}}$, which is deduced by the Einstein formula. Under the EMD method in our work, the size of the above sample also can fully meet the requirements of its thermal conductivity evaluation [31].

3.1. Effect of defects

Next, we introduced three different types of defects, single vacancy, double vacancies and SW defects, in the above pristine graphene sample. Each defect contains the following nine different concentrations: 0.3%, 0.6%, 0.9%, 1.2%, 1.5%, 2.1%, 3%, 6% and 10%. For each concentration of three different defect types, we constructed three different atomic models with defects in a random distribution. Three independent simulations with different initial velocities were performed for each model, and the average of the thermal conductivity was taken as the final calculation result. This statistical average processing method can effectively reduce the influence of the specific distribution position of the defect on the thermal conductivity calculation result, so that the defect type and defect concentration are the focus of this study. For the defective graphene structure, in order to avoid structural instability during the simulation, we chose the simulation time step of 0.5*fs*. And the other details of the simulations are identical to those of the previous pristine graphene.

The calculated normalized thermal conductivity of different defective graphene with different defect concentrations

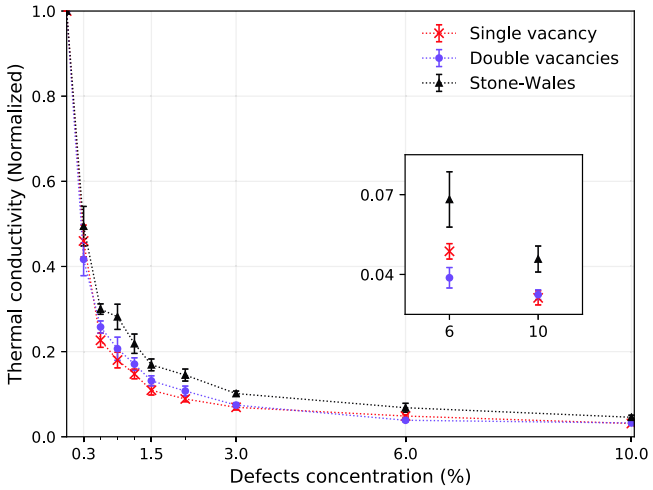

Figure 4. Normalized thermal conductivity calculation results for different defect concentrations after introducing three different kinds of defects into the pristine graphene of 20 nm × 20 nm. There are nine kinds of defect concentration: 0.3%, 0.6%, 0.9%, 1.2%, 1.5%, 2.1%, 3.0%, 6.0%, and 10%, which can clearly describe the changes of thermal conductivity.

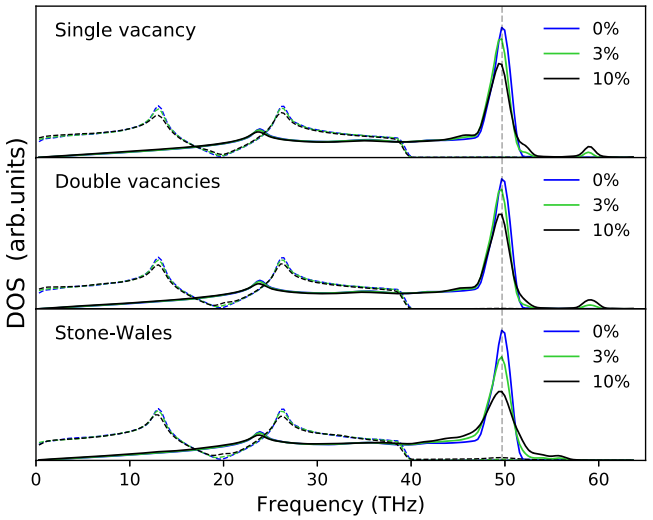

Figure 5. Calculated DOS of pristine graphene and three defective graphene at concentrations of 3% and 10% (The solid line represents the in-plane part, and the dashed line represents the out-of-plane part. It is not difficult to find that the low frequency phonon vibration mainly comes from the out-of-plane part, which is also the main source of thermal conductivity.)

at 300 K are shown in figure 4. Firstly, the effect of defect concentration on the thermal conductivity of graphene is discussed. It is not difficult to find that the thermal conductivity of graphene with three kinds of defects has almost the same tendency with the change of defect concentration: all of them reveal drastic decline with the increase of defect concentration. At a defect concentration of only 0.3%, the thermal conductivity value of defective graphene shows a large decrease, about half of the original. When the defect concentration increases to about 3%, the thermal conductivity value of defective graphene is reduced by almost an order of magnitude. And as the defect concentration increases, the declining rate in the thermal conductivity value is generally less. It means that at large defect concentrations, the slight difference in defect concentration does not have much effect on the thermal conductivity of defective graphene, which is meaningful for the defects engineering of graphene. Under the condition of satisfying the thermal conductivity requirement with the large concentration defect, the concentration condition can be appropriately relaxed to adjust other properties of graphene to achieve the overall application purpose. Then, longitudinal comparison of different types of defective graphene is carried. Due to the similar defect formation styles, the thermal conductivity of defective graphene containing single vacancy and double vacancies defects has the quite small gap. However, the SW defect is the only one of the three defect types that does not involve atomic loss. The thermal conductivity of graphene containing this defect is significantly higher than the other two in all defect concentrations.

In order to further understand the fundamental mechanism of the weakening of graphene thermal conductivity caused by defects, we have studied from the perspective of phonon. At the defect concentration of 3% and 10%, we calculated the phonon density of states (DOS) of the above three kinds of defective graphene, which describes the relationship between the phonon mode and the frequency. The DOS of the same size of the pristine graphene was also calculated as a comparison term. In the equilibrium simulation process of 100*ps*, the velocity of carbon atoms was recorded every 5*fs*, and the DOS was obtained by performing the following Fourier transform on the velocity auto-correlation function:

$$DOS_\alpha(\omega) = \int_{-\infty}^{+\infty} \langle v_\alpha(t) v_\alpha(0) \rangle e^{-2\pi i \omega t} dt \ (\alpha = x, y, z), \quad (4)$$

where ω is the frequency, t is the correlated time of velocity auto-correlation function $\langle v_\alpha(t) v_\alpha(0) \rangle$ of carbon atoms.

In the above formula, the thermal conductivity of graphene is mainly derived from the contributions of three acoustic modes: In-plane transverse acoustic (TA) mode along the x-direction, in-plane longitudinal acoustic (LA) mode along the y-direction, and out-of-plane bending acoustic (ZA) mode along the z-direction. In the square graphene studied in this paper, the difference between the in-plane acoustic modes TA and LA is negligible, and we average the two as a unified in-plane acoustic mode.

It is revealed that the intervention of three defects has a significant effect on graphene in both in-plane and out-of-plane acoustic modes in figure 5. Firstly, we focus on the in-plane part, which is plotted by solid lines. Due to the intervention of defects, the DOS of graphene has a significant damping effect at the peak near 50 THz. As the concentration of defects increases, the attenuation of DOS becomes more and more obvious. The out-of-plane DOS is wider around the two frequency peaks located in the low frequency band of less than 30 THz, and the peak value is reduced. These changes mean a decrease in the lifetime of the phonon [45], thus causing a decrease in the thermal conductivity of the graphene.

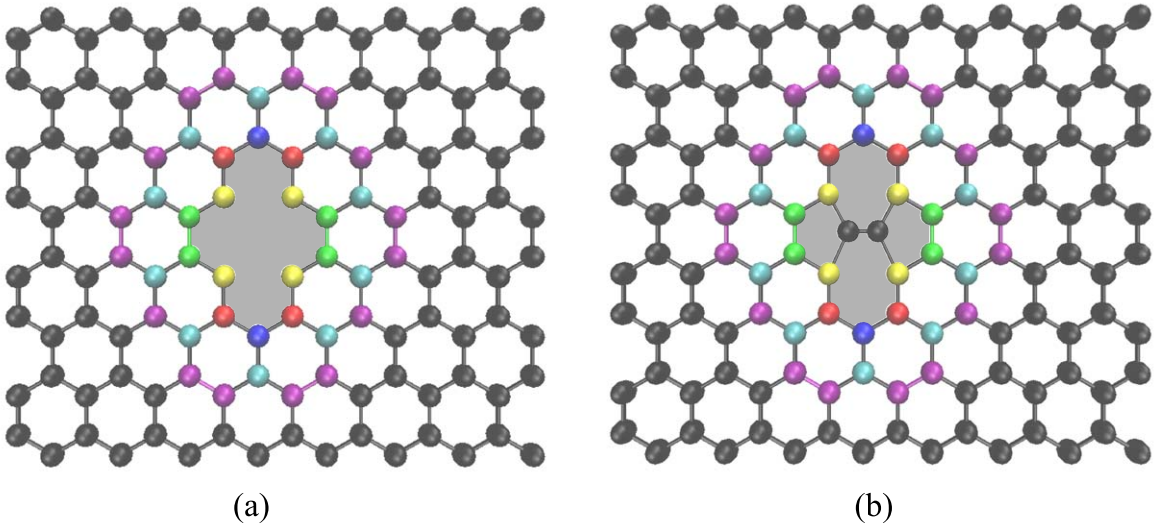

Figure 6. Schematic illustration of defective graphene containing a double vacancies (a) and an SW defect (b) respectively. The shaded area represents the location of the single topological defect, and the balls in different colors around represent the six types of carbon atoms symmetrically distributed around the defect.

It is revealed that the effects of single vacancy defects and double vacancies defects on the DOS of graphene are close. This also confirms that these two types of defective graphene have almost the same thermal conductivity at different defect concentrations. In contrast, defective graphene containing SW defects has a more severely weakened in high-frequency mode. However, the low frequency band below 30 THz is less affected than the other two types of defective graphene, which is characterized by weaker changes of acoustic mode below 4 THz and the out-of-plane acoustic mode at two peaks. It is generally believed that the main contribution of thermal conductivity comes from low-frequency phonons [45, 46], so the above differences lead to the thermal conductivity of SW defective graphene always exceed the other two at the same defect concentration.

Then, we explored the specific impact of double vacancies defect and SW defect on the thermal conductivity of graphene, since the difference between single vacancy and double vacancies is negligible. We calculated the DOS of carbon atoms near the two defects for comparative analysis. To simplify the analysis, we used the following simplified model with a single defect to calculate and discuss the vibrational dynamics of carbon atoms at different locations around the defect, as figure 6 shown. Considering the symmetry of the defect itself, the DOS calculation results for each position are averaged from the equivalent carbon atoms.

As shown in figure 7, for the carbon atoms near the defect, it is not difficult to find that the calculated DOS is affected to varying degrees. The four positions (a)–(d) are carbon atoms that directly constitute defect, and (e)–(f) represent atoms around the defect. Comparing the calculated DOS of a carbon atom in pristine graphene, the DOS of the six positions is greatly affected in the low frequency range of less than 4 THz, which also means that the defect severely weaken the surrounding phonons with low frequency. However, the performance at the high frequency peak near 50 THz

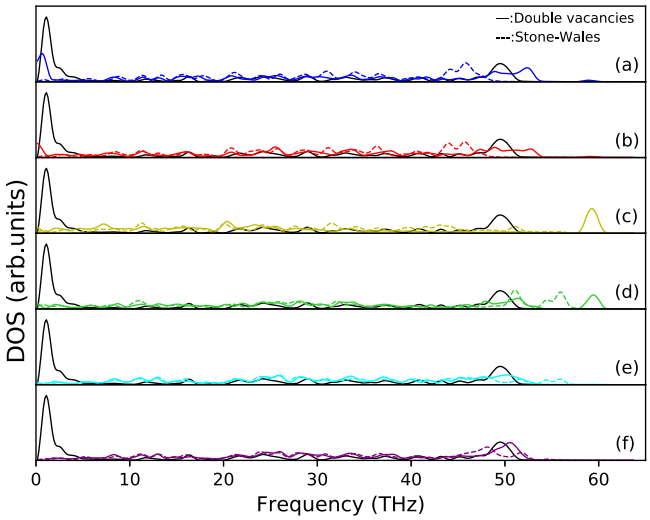

Figure 7. The relationship between the calculated DOS and the frequency of the pristine graphene carbon atom (plotted by the solid black line), the double vacancies defect (plotted by the solid color line) and the SW defect (plotted by the colored dashed line); The six calculation results correspond to the DOS of carbon atoms identified by different colors in figure 6, where the color of the line is in one-to-one correspondence with the atomic identification color. The color in (a)–(f) are blue, red, yellow, green, cyan and purple respectively.

is different. Since high-frequency phonons contribute little to the thermal conductivity of graphene, we do not regard it as the focus of research.

For the carbon atoms (e) and (f) around the defects, it is shown that the vibration state of them is still affected, even if the high frequency peaks is relatively close to the pristine graphene carbon atoms. It means that the existence of defects not only affects the atomic vibrations that make up the defects, but also affects the atoms around the defects. These can lead to local acoustic mismatch, resulting in phonon-defect scattering, which is the root cause of the significant

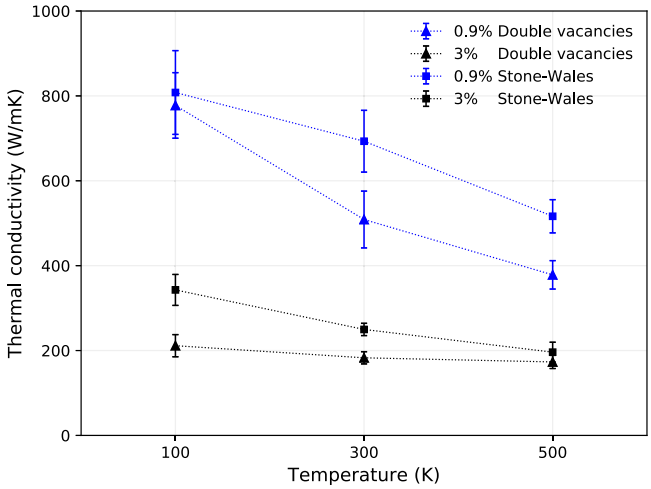

Figure 8. Thermal conductivity of defective graphene with double vacancies and SW defects at 0.9% and 3% concentrations under three temperatures of 100, 300 and 500 K, which basically cover all application scenarios of graphene. (Among them, the difference in concentration is distinguished by different colors, and the difference in defect types is distinguished by different shapes.)

decrease in graphene thermal conductivity. Furthermore, in defective graphene with large defect concentrations, it is inevitable that two or more independent defect distances are so close that their respective areas of influence may overlap. This allows the same carbon atom to be affected by different independent defects simultaneously, which will further aggravate the phonon scattering effect.

3.2. Effect of temperature

In addition, we also studied the effect of temperature on the thermal conductivity of defective graphene, which is an indispensable factor in the influence of lattice vibration. Under three temperature conditions of 100 K, 300 K and 500 K, double vacancies and SW defective graphene with a concentration of 0.9% and 3% and a size of 20 nm × 20 nm were discussed here. The three temperature conditions correspond to low temperature, room temperature, and high temperature, covering almost all possible application scenarios of defective graphene. As shown in the calculation results presented in figure 8, as the temperature increases, the thermal conductivity of defective graphene generally decreases. This is due to the increase in temperature which intensifies the vibration of the crystal lattice within the structure, thereby enhancing phonon–phonon scattering, which is a major contribution of thermal resistance. Comparing the data of the two different colors in figure 8, it represents the thermal conductivity of defective graphene at different concentrations. Graphene with high defect concentration (data plotted in black) is less sensitive to temperature changes. It is revealed that phonon-defect scattering plays a major role in the contribution of thermal resistance in graphene with higher defect concentration.

Attention is paid to two kinds of defective graphene with a low concentration of 0.9% in 100 K, which is plotted in blue in figure 8. Due to the low defect content of the two graphene, the difference between the two defect effects is relatively minor in the overall graphene. On this basis, the weak lattice vibration under the low temperature further weakens the difference in defect types. This resulted in that the two types of defective graphene with a concentration of 0.9% had almost the same thermal conductivity at a temperature of 100 K.

However, for higher concentration, the thermal conductivity of both types of defective graphene is greatly weakened. At higher and lower concentrations of 300 K, the difference in thermal conductivity between the two types of defective graphene is approximately 184.47 W mK^{-1} and 66.84 W mK^{-1}, respectively. The former is almost three times the latter. It is shown that under the condition of higher defect concentration, the difference in thermal conductivity caused by the difference in defect type itself is less. Further, the high temperature makes the influence of phonon–phonon scattering on thermal conductivity increases, which weakens the phonon-defect scattering to a certain extent, resulting in the thermal conductivity results of two kinds of defective graphene with a concentration of 3% at 500 K are very close.

To sum up the above discussion, defect and temperature are two important factors to affect thermal resistance, and these two restrict each other and affect each other, and together determine the thermal conductivity of defective graphene.

4. Conclusion

In summary, we studied the thermal transport properties of defective graphene through molecular dynamics simulation based on GPU. It has been found that the intervention of topological defects has a great weakening effect on the thermal conductivity of graphene. The defect concentration is roughly negatively correlated with the thermal conductivity of graphene, and as the concentration increases, the thermal conductivity decreases more and more slowly. At the same defect concentration, the thermal conductivity of graphene containing single vacancy and double vacancies defects is very similar and is always less than that of graphene containing SW defects. The calculated DOS results show that the difference in the attenuation of out-plane low-frequency phonons is the root cause of the difference in thermal conductivity. The high temperature will aggravate the lattice vibration and increase the phonon–phonon scattering term, which will reduce the thermal conductivity of the defective graphene. In addition, this paper also explores the possible constraints between the phonon–phonon scattering term and the phonon-defective scattering term. The work has comprehensively studied the thermal transport properties of defective graphene, and these findings tend to have possible extension to the application of graphene defect engineering in the field of thermal management and thermal design of nanomaterials.

Acknowledgments

The authors are grateful for support from the National Natural Science Foundation of China (11772130,11972160) and Guangdong Basic and Applied Basic Research Foundation (2019A1515011900).

ORCID iDs

Qiang Han https://orcid.org/0000-0002-9972-461X

References

[1] Ravindra Kempaiah A C and Maheshwari V 2011 Graphene as cellular interface electromechanical coupling with cells *ACS Nano* **5** 6025–31
[2] Kucsko G, Maurer P C, Yao N Y, Kubo M, Noh H J, Lo P K, Park H and Lukin M D 2013 Nanometre-scale thermometry in a living cell *Nature* **500** 54–8
[3] He X, Liu F, Lin F and Shi W 2019 Investigation of terahertz all-dielectric metamaterials *Opt. Express* **27** 13831–44
[4] Butler S Z 2013 Progress, challenges, and opportunities in two-dimensional materials beyond graphene *ACS Nano* **7** 2898
[5] Xu M, Liang T, Shi M and Chen H 2013 Graphene-like two-dimensional materials *Chem. Rev.* **113** 3766–98
[6] Habe T and Koshino M 2015 Spin-dependent refraction at the atomic step of transition-metal dichalcogenides *Phys. Rev.* B **91** 201407
[7] Tran V, Soklaski R, Liang Y and Yang L 2014 Layer-controlled band gap and anisotropic excitons in few-layer black phosphorus *Phys. Rev.* B **89** 235319
[8] Shi C, He X, Peng J, Xiao G, Liu F, Lin F and Zhang H 2019 Tunable terahertz hybrid graphene-metal patterns metamaterials *Opt. Laser Technol.* **114** 28–34
[9] He X, Lin F, Liu F and Zhang H 2019 Investigation of phonon scattering on the tunable mechanisms of terahertz graphene metamaterials *Nanomaterials* **10** 39
[10] He X, Liu F, Lin F, Xiao G and Shi W 2019 Tunable MoS2 modified hybrid surface plasmon waveguides *Nanotechnology* **30** 125201
[11] Novoselov K S, Geim A K, Morozov S V, Jiang D, Zhang Y, Dubonos S V, Grigorieva I V and Firsov A A 2004 Electric field effect in atomically thin carbon films *Science* **306** 666–9
[12] Allen M J 2010 Honeycomb carbon: a review of graphene *Chem. Rev.* **110** 132–45
[13] Bae M H, Ong Z Y, Estrada D and Pop E 2010 Imaging, simulation, and electrostatic control of power dissipation in graphene devices *Nano Lett* **10** 4787–93
[14] Pulizzi F, Bubnova O, Milana S, Schilter D, Abergel D and Moscatelli A 2019 Graphene in the making *Nat. Nanotechnol.* **14** 914–8
[15] Cai W, Moore A L, Zhu Y, Li X, Chen S, Shi L and Ruoff R S 2010 Thermal transport in suspended and supported monolayer graphene grown by chemical vapor deposition *Nano Lett.* **10** 1645–51
[16] Balandin A A 2008 Superior thermal conductivity of single-layer graphene *Nano Lett.* **8** 902–7
[17] Chen S 2011 Raman measurements of thermal transport in suspended monolayer graphene ofvariable sizes in vacuum and gaseous environments *ACS Nano* **5** 321–8
[18] Li Z 2011 Low-temperature growth of graphene by chemical vapor deposition using solid and liquid carbon sources *ACS Nano* **5** 3385–90
[19] Berger C 2004 Ultrathin epitaxial graphite: 2D electron gas properties and a route toward graphene-based nanoelectronics *J. Phys. Chem.* B **108** 19912–6
[20] Terrones M, Botello-Méndez A R, Campos-Delgado J, López-Urías F, Vega-Cantú Y I, Rodríguez-Macías F J, Elías A L, Muñoz-Sandoval E, Cano-Márquez A G and Charlier J-C 2010 Graphene and graphite nanoribbons: morphology, properties, synthesis, defects and applications *Nano Today* **5** 351–72
[21] Fan Z, Pereira L F C, Hirvonen P, Ervasti M M, Elder K R, Donadio D, Ala-Nissila T and Harju A 2017 Thermal conductivity decomposition in two-dimensional materials: application to graphene *Phys. Rev.* B **95** 144309
[22] Schelling P K, Phillpot S R and Keblinski P 2002 Comparison of atomic-level simulation methods for computing thermal conductivity *Phys. Rev.* B **65** 144306
[23] Ghasemi H, Rajabpour A and Akbarzadeh A H 2018 Tuning thermal conductivity of porous graphene by pore topology engineering: comparison of non-equilibrium molecular dynamics and finite element study *Int. J. Heat Mass Transfer* **123** 261–71
[24] Cui L, Zhang Y, Du X and Wei G 2017 Computational study on thermal conductivity of defective carbon nanomaterials: carbon nanotubes versus graphene nanoribbons *J. Mater. Sci.* **53** 4242–51
[25] Wei Z, Ni Z, Bi K, Chen M and Chen Y 2011 In-plane lattice thermal conductivities of multilayer graphene films *Carbon* **49** 2653–8
[26] Noshin M, Khan A I, Navid I A and Subrina S 2017 Thermal transport in defected armchair graphene nanoribbon: a molecular dynamics study *TENCON 2017 - 2017 IEEE Region 10 Conference* pp 2600–3
[27] Plimpton S 1993 Fast parallel algorithms for short-range molecular dynamics *J. Comput. Phys.* **117** 1–19
[28] Dong Y, Meng M, Groves M M, Zhang C and Lin J 2018 Thermal conductivities of two-dimensional graphitic carbon nitrides by molecule dynamics simulation *Int. J. Heat Mass Transfer* **123** 738–46
[29] Dong R-Y, Dong Y, Li Q and Wan C 2020 Ballistic-diffusive phonon transport in cellulose nanocrystals by ReaxFF molecular dynamics simulations *Int. J. Heat Mass Transfer* **148** 119155
[30] Diao C, Dong Y and Lin J 2017 Reactive force field simulation on thermal conductivities of carbon nanotubes and graphene *Int. J. Heat Mass Transfer* **112** 903–12
[31] Fan Z, Pereira L F C, Wang H-Q, Zheng J-C, Donadio D and Harju A 2015 Force and heat current formulas for many-body potentials in molecular dynamics simulations with applications to thermal conductivity calculations *Phys. Rev.* B **92** 094301
[32] Boone P, Babaei H and Wilmer C E 2019 Heat flux for many-body interactions: corrections to LAMMPS *J. Chem. Theory Comput.* **15** 5579–87
[33] Jász Á, Rák Á, Ladjánszki I and Cserey G 2019 Classical molecular dynamics on graphics processing unit architectures *WIREs Comput. Mol. Sci.* **10** e1444
[34] Fan Z, Siro T and Harju A 2013 Accelerated molecular dynamics force evaluation on graphics processing units for thermal conductivity calculations *Comput. Phys. Commun.* **184** 1414–25
[35] Green M S 1954 Markoff random processes and the statistical mechanics of time-dependent phenomena. II. irreversible processes in fluids *J. Chem. Phys.* **22** 398
[36] Kubo R 1957 Statistical mechanical theory of irreversible processes. I. General theory and simple applications to magnetic and conduction problems *J. Phys. Soc. Japan* **12** 570–86
[37] Lindsay L and Broido D A 2010 Optimized Tersoff and Brenner empirical potential parameters for lattice dynamics and phonon thermal transport in carbon nanotubes and graphene *Phys. Rev.* B **81** 205441

[38] Mortazavi B and Ahzi S 2013 Thermal conductivity and tensile response of defective graphene: a molecular dynamics study *Carbon* **63** 460–70
[39] Mortazavi B, Fan Z, Pereira L F C, Harju A and Rabczuk T 2016 Amorphized graphene: a stiff material with low thermal conductivity *Carbon* **103** 318–26
[40] Zhang H, Lee G and Cho K 2011 Thermal transport in graphene and effects of vacancy defects *Phys. Rev.* B **84**
[41] Haskins J, Kınacı A, Sevik C, Sevinçli H, Cuniberti G and Çağın T 2011 Control of thermal and electronic transport in defect-engineered graphene nanoribbons *ACS Nano* **5** 3779–87
[42] Kinaci A, Haskins J B and Cagin T 2012 On calculation of thermal conductivity from Einstein relation in equilibrium molecular dynamics *J. Chem. Phys.* **137** 014106
[43] Gill-Comeau M and Lewis L J 2015 Heat conductivity in graphene and related materials: a time-domain modal analysis *Phys. Rev.* B **92** 195404
[44] Lindsay L, Li W, Carrete J, Mingo N, Broido D A and Reinecke T L 2014 Phonon thermal transport in strained and unstrained graphene from first principles *Phys. Rev.* B **89** 155426
[45] Turney J E, Landry E S, McGaughey A J H and Amon C H 2009 Predicting phonon properties and thermal conductivity from anharmonic lattice dynamics calculations and molecular dynamics simulations *Phys. Rev.* B **79** 064301
[46] Ladd A J C, Moran B and Hoover W G 1986 Lattice thermal conductivity: a comparison of molecular dynamics and anharmonic lattice dynamics *Phys. Rev.* B **34** 5058–64